EUROPEAN ORGANIZATION FOR NUCLEAR RESEARCH (CERN)

Addendum to Technical Proposal

A Facility to Search for Hidden Particles (SHiP) at the CERN SPS

The SHiP Collaboration

CERN-SPSC-2015-040 / SPSC-P-350-ADD-2
19/10/2015

Abstract

With the Technical Proposal (TP) submitted to the SPSC committee in April 2015 [1], the SHiP collaboration declared its interest in proceeding towards a comprehensive design study phase with the aim of preparing for the Technical Design Reports pending an approval by the CERN committees. Following the recommendation by the SPSC, it has been decided to complement the TP with this addendum that provides an update of the key aspects for the review of the SHiP project.

Contents

Executive Summary

With the Technical Proposal (TP) submitted to the SPSC committee in April 2015 [1], the SHiP collaboration declared its interest in proceeding towards a comprehensive design phase with the aim of preparing for the Technical Design Reports (TDR) for the SHiP detector located at a new general purpose facility at the CERN SPS. Following the recommendation by the SPSC, it has been decided to complement the TP with this addendum which provides an update of the key aspects for the review of the SHiP project.

As indicated by the experimental results in flavour physics, searches for charged lepton flavour violation, and electric dipole moment of the electron, the scale of new physics is well above the direct reach at existing or planned accelerators, $\Lambda > 10^3$ TeV, in BSM models with not suppressed couplings. SHiP is an ideal instrument to search for new superweakly interacting particles with masses below $O(10)$ GeV at the presence of no competing SM processes.

Based on the increased statistics of MC data samples, Sections 1 and 2 summarize the recent progress in understanding the backgrounds and the sensitivity for representative physics channels. The updated background estimate firmly confirms the TP estimate of zero expected events. Furthermore, while the TP only considered the signal yield from primary proton interactions, a recent study has shown that the production of charm and beauty in cascade processes increases the yield by 40-50% including acceptance effects. This applies to all types of hidden particles produced in decays of charm and beauty hadrons, and the production of tau neutrinos. All sensitivity plots will be updated once the effect has been implemented in the full MC.

Section 3 provides a comparison of the sensitivity reach of the SHiP experiment with a hypothetical SHiP-like experiment, optimized for the available beam energy at FNAL and at JPARC. Assuming that the beam time is fully dedicated, and assuming that the challenge of the target and the slow extraction is solved, an experiment at FNAL could reach similar sensitivity to HNLs and dark photons. The sensitivity to dark scalars and tau neutrino physics is significantly worse. The experiment at JPARC is not competitive due to the very low beam energy. A brief comparison with other existing and planned experiments is also given in Section 3. The SHiP sensitivity reach greatly exceeds the sensitivity of other projects, in particular for HNLs, dark scalars and tau neutrinos.

Finally Section 4 presents an update of the schedule and the resources for the preparation of the SHiP detector and the facility. It also provides details on the resources required from CERN during the comprehensive design phase, and a list of the key milestones to be addressed. The new schedule and cost profile take into account the recently updated accelerator schedule and the HL-LHC project plan. It reschedules the civil engineering of the TDC2 junction cavern and the first section of the SHiP beam line to LS3 and changes the order of the other work packages. This relaxes signicantly the design and the preconstruction phase, and it allows a significant shift in the funding required from CERN by about two years. At the same time, it allows maintaining the start of data taking as soon as SPS resumes operation after LS3. The milestones related to both the facility and the detector can be met with a modest investment during the next few years. Many of the milestones related to the facility are of general interest beyond SHiP. The key milestones related to the detector concern optimizations of the experiment in terms of the global layout and the detector geometries, and hence provide grounds for significant cost optimizations. No attempt has been made yet to update the costs of the detector and the facility in view of these optimizations.

Chapter 1

Updated background estimates

An accurate evaluation of backgrounds is a critical aspect of the SHiP physics performance. Since the TP, the MC data samples were increased by factors between ~ 2 and 10, depending on the background channels. In addition, the selection criteria have now been made uniform across background and signal channels. This allows a reasonable update of the backgrounds for all the sources presented in the TP, namely:

- neutrino scattering in the vicinity of the decay volume;
- muon inelastic scattering in the vicinity of the decay volume;
- muon combinatorial background;
- cosmic muon background;

The updated estimates of these backgrounds are presented together with a brief reminder of the evaluation strategy, including a few additional distributions and tables missing in the TP.

1.1 Selection criteria

The selection criteria used in all background and signal channels may be divided in four main categories:

- *fiducial requirements:* each reconstructed event should have a vertex located in the fiducial volume, at least 20 cm downstream of the straw veto station and at least 20 cm upstream of the first tracker station. It is contained in the elliptical cross-section of the vessel, with 1 cm tolerance at the border. The tracks forming the candidate must be fully contained in the vessel, with 1 cm tolerance at the border.
- *kinematic requirements:* the event comprises two reconstructed tracks of opposite charge with at least 1 GeV/c momentum, a track quality of $\chi^2/N_{\rm DOF} < 5$, a number of degrees of freedom $N_{\rm DOF} > 25$ in the Hidden Sector (HS) straw tracker. The last requirement ensures a sufficient amount of hits in each tracking station. Tracks not crossing all the four

tracking stations are not considered. The distance of closest approach of the tracks must be $DOCA < 1$ cm[1]. The impact parameter of the reconstructed particle with respect to the target must be $IP < 10$ cm for fully reconstructed final states[2], while it is relaxed to $IP < 2.5$ m for final states with nondetected neutrinos.

- *Coincidence requirement:* assumes that the two tracks arrive at the HS spectrometer with a time difference < 340 ps, corresponding to $\sim \sqrt{2} \times 2.5\ \sigma_t$ where σ_t is the time resolution of the timing detector;

- *veto requirements:* assume that at least one of the veto detectors (Upstream Veto, Straw Veto, RPC in the neutrino detector, or Surround Veto Tagger) is fired.

In the following, these sets of cuts are applied to the different background components and their rejection factor is evaluated. In Chapter 2 the same selection criteria are applied to two representative signal channels and the corresponding efficiencies are evaluated.

1.2 Neutrino-induced background

The flux of neutrinos is estimated to be $1.0 \cdot 10^{11}$ per proton spill with momentum between 2 GeV/c and 100 GeV/c (average $p \sim 5$ GeV/c) and polar angle within 100 mrad, while the corresponding flux of anti-neutrinos is $7.3 \cdot 10^{10}$.

Neutrinos interacting with the material in the vicinity of the decay volume can produce particles that enter the vacuum vessel and mimic the signal. This background is efficiently rejected by the veto systems as deep inelastic scattering of neutrinos typically produce events with large multiplicity. Moreover these events in general do not have a vertex reconstructed inside the fiducial volume, do not point to the target and have a very poor track quality, hence they are effectively reduced by applying the kinematic cuts.

The interactions of neutrinos with material are generated by the GENIE package using the neutrino spectrum, shown in Figure 1.1, as it is predicted by FairSHiP. We expect $\sim 10^7$ neutrino interactions for $N_{\text{pot}} = 2{\cdot}10^{20}$ and a factor ~ 3 less for anti-neutrinos due to their lower flux and lower cross-section. Each neutrino event is assigned a statistical weight corresponding to the ratio of the generated events in a given momentum range compared to those expected for 2×10^{20} protons on target in the same momentum range. With respect to the TP the neutrino sample has been increased by about a factor of two in the momentum interval between 2 and 10 GeV/c.

The results are shown in Table 1.1 for neutrino interactions and in Table 1.2 for anti-neutrino interactions. Most of the neutrino interactions originate in the tau neutrino detector and in the walls of the vacuum vessel. A not negligible fraction interacts in the vessel lids and in the material of the tracking system, while no background events are generated in neutrino interactions with the cavern walls.

The vacuum level of 10^{-3} mbar in the decay volume has been designed to produce less than one interaction in the residual air for the $2{\cdot}10^{20}$ protons on target. This requirement

[1] the average DOCA for signal events is ~ 3.6 mm

[2] The average IP for fully reconstructed signal events is 1.65 cm. This should be folded together with the beam sweep on the target of 3 cm radius.

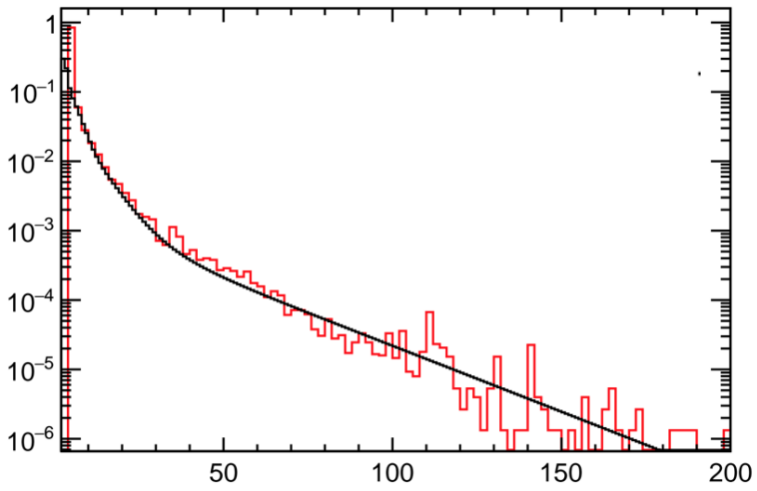

Figure 1.1: Momentum spectrum (in GeV/c) of neutrinos after the hadron absorber. The red histogram corresponds to the momentum of all neutrinos, while the black curve parametrizes the momentum spectrum of neutrinos within the SHiP acceptance.

is very conservative since most of these background events do not have two charged particles that traverse the detector. In addition an efficient rejection of this background is achieved by veto and selection requirements. Considering reconstruction, selection and vetos the expected number of background events from neutrinos scattering in the decay volume is $O(10^{-6})$. This will allow relaxing the vacuum requirements in the decay volume. It will be studied and optimized during the comprehensive design phase.

The fiducial and kinematic requirements alone are able to reduce the neutrino induced background down to < 0.2 events in $2 \cdot 10^{20}$ protons on target, corresponding to a reduction factor of $\sim 2 \cdot 10^{-8}$. The veto requirements alone introduce a reduction factor of $6 \cdot 10^{-6}$. Consistent results are observed for anti-neutrinos. Table 1.3 shows step-by-step the effect of the pre-selection cuts described in Section 1.1 and the signal selection cuts described in Section 2.2 on the neutrino induced background. This should be compared with the effect on the signal efficiencies shown in Table 2.1 and 2.2.

After applying veto, fiducial and kinematic criteria no background events are left. Hence, an upper limit at 90% CL is set for the three momentum intervals corresponding to the three different statistical weights of UL(90% CL) $= -\ln(0.1)/\text{weight}$. Results are summarized in Table 1.4 for neutrinos and in Table 1.5 for anti-neutrinos. It should be emphasized that the sample of neutrinos was generated for the TP [1], while the sample of anti-neutrinos has been generated with an updated version of the simulation[3]. However, for both simulation settings no background events survive the selection and the veto criteria. Actual values of the upper limits depend on the available Monte Carlo samples and are expected to further decrease with increased statistics.

[3]The principal difference in the two simulations is the addition of the yokes of the magnet for the muon spectrometer used in the tau neutrino detector. This simulation difference is visible in the number of anti-neutrino interactions in the Tau neutrino detector in Table 1.2. However, the effect has negligible impact on the number of background candidates since these are mostly outside of the acceptance.

Table 1.1: Number of neutrino interactions produced in the material and with at least two reconstructed tracks in the detector for $N_{pot} = 2 \cdot 10^{20}$. The first column shows the origin of the neutrino interaction, the second column shows the number of interactions with at least two charged tracks reconstructed in the HS spectrometer. The numbers of remaining events after applying the veto and the selection requirements are shown in the third and fourth column, respectively. The relative fraction of neutrino interactions with different detector elements for reconstructed/not-vetoed/selected events is indicated in brackets. It should be noticed that the number of selected events does not include any veto. After applying selection and veto no events survive.

Detector	Reconstructed (%)	Not vetoed (%)	Selected (%)
Tau neutrino detector	17957.4 (57.6)	4.3 (4.9)	0.2 (100.0)
Vessel lids	281.6 (0.9)	0.0 (0.0)	0.0 (0.0)
Vessel walls	12556.9 (40.3)	37.5 (43.0)	0.0 (0.0)
Straw veto	0.0 (0.0)	0.0 (0.0)	0.0 (0.0)
Tracking system	362.2 (1.2)	45.5 (52.1)	0.0 (0.0)
Cavern walls	0.0 (0.0)	0.0 (0.0)	0.00 (0.00)
Decay volume (vacuum)	$5.8{\cdot}10^{-3}$	$0.2{\cdot}10^{-3}$	$2{\cdot}10^{-6}$
Others	4.1 (0.0)	0.0 (0.0)	0.00 (0.00)
Total	**31162.1**	**87.3**	**0.21**

Table 1.2: Same as Table 1.1 for anti-neutrino interactions.

Detector	Reconstructed (%)	Not vetoed (%)	Selected (%)
Tau neutrino detector	7023.8 (63.6)	1.2 (2.6)	0.0 (0.0)
Vessel lids	104.9 (0.9)	0.0 (0.0)	0.0 (0.0)
Vessel walls	3778.3 (34.2)	22.9 (48.0)	0.0 (0.0)
Straw veto	0.0 (0.0)	0.0 (0.0)	0.0 (0.0)
Tracking system	136.3 (1.2)	23.6 (49.5)	0.0 (0.0)
Cavern walls	0.1 (0.0)	0.0 (0.0)	0.00 (0.00)
Decay volume (vacuum)	$1.8{\cdot}10^{-3}$	$0.1{\cdot}10^{-3}$	$3{\cdot}10^{-6}$
Others	2.9 (0.0)	0.0 (0.0)	0.00 (0.00)
Total	**11046.3**	**47.8**	**0.00**

Table 1.3: Efficiencies corresponding to the different selection criteria applied to the neutrino induced background. The efficiency of each cut is computed with respect to the preceding cut. The second column (Entries) shows the number of unweighted events, while the third column (Events) shows the number of weighted events. Reconstructed events are defined as the number of candidate with at least two opposite sign tracks forming a vertex. This table uses the neutrino sample only.

Selection	**Entries**	**Events / $2{\cdot}10^{20}$ p.o.t.**	**Selection efficiency**
Events reconstructed	91125	31162	-
1 HNL Candidate	70049	24561	78.8 %
Vtx in fiducial vol.	14700	5124	20.9 %
Tracks in fiducial vol.	11287	3868	75.5 %
N.d.f > 25	6326	1965	50.8 %
DOCA $<$ 1cm	832	311	15.9 %
χ^2 / N.d.f < 5	831	311	99.9 %
Daughters $P > 1$ GeV	589.0	202	65.1 %
IP $<$ 10cm ($<$ 2.5m)	1 (311)	0.2 (76.8)	0.1 (38.0%) %
Events not vetoed	0	0.0	0.0 %

Table 1.4: Upper limit at 90% CL on the number of neutrino induced background events as derived from the full simulation. The sample is divided in three momentum regions. The *statistical weight* is the ratio between the generated samples and the expected number of interactions for $2{\cdot}10^{20}$ protons on target.

Bkg source	Stat. weight	Expected background (U.L. 90% CL)
ν (2.0 $<$ p $<$ 4.0 GeV/c)	1.42	1.62
ν (4.0 $<$ p $<$ 10.0 GeV/c)	2.53	0.91
ν (p $>$ 10.0 GeV/c)	3.02	0.76

Table 1.5: Upper limit at 90% CL on the number of anti-neutrino background events as derived from the full simulation. The sample is divided in three momentum regions. The *statistical weight* is the ratio between the generated samples and the expected number of interactions for $2{\cdot}10^{20}$ protons on target.

Bkg source	Stat. weight	Expected background (U.L. 90% CL)
$\bar{\nu}$ (2.0 $<$ p $<$ 4.0 GeV/c)	2.39	0.96
$\bar{\nu}$ (4.0 $<$ p $<$ 10.0 GeV/c)	2.76	0.83
$\bar{\nu}$ (p $>$ 10.0 GeV/c)	6.79	0.34

1.3 Muon inelastic background

In the updated estimate of the background from muon inelastic scattering, the preselection is now the same as in the studies of the other backgrounds. The main change is that the impact parameter cut has been relaxed to $2.5\,m$, and the cut on the fiducial volume is tighter to take into account the vertex resolution. In addition, the muon spectrometer of the ν_τ has been added as veto for muon interactions in front of the decay vessel, and the requirement of oppositely charged tracks to form a vertex has been dropped to increase the statistics of potential background events. After the TP, it was noticed that muons entering the decay vessel were not followed properly in Geant4 due to the way in which the muon background was being simulated. As a consequence, the incoming muons did not produce any signals in the veto detectors. This has been corrected and results are also shown below in the case that only veto signals are used from either the incoming muons or from the particles produced in the muon interaction with the material.

The origin of the background events has been studied in more detail. Background candidates from V^0 decays are shown in Figure 1.2. These events are very efficiently rejected by the veto counters wich are either triggered by the charged particles produced together with the V^0 particles in the muon inelastic interaction or by the detection of the incoming muon. It can be safely assumed that the veto efficiencies for the incoming muon and for the particles produced in the muon interaction factorize. Figure 1.3 shows the impact parameter distribution versus the invariant mass for the remaining background candidates with only two tracks in the final state. All these events can be removed by applying the veto cuts, also shown in Figure 1.3.

The results of the different cuts on muon inelastic background are summarized on Table 1.6. The request that none of the veto counters is fired brings the background to zero. Hence we can set an upper limit for 2×10^{20} protons on target at 90% CL, $UL(90\%CL) < -\ln(0.1)/w = 4.6$. In addition, assuming factorization of the veto efficiency for the incoming muon and for the particles produced in the muon interaction, pushes the background limit to $UL(90\%CL) < 0.005$.

Currently, the veto decisions are derived from counting hits in the veto detectors globally. However, there is a strong correlation between the reconstructed tracks and the muon interaction point, as shown in Figure 1.4. In order to be more robust against noise hits, the future approach will be based on counting hits around the track extrapolation.

Another source of background events originate from pairs of tracks with very small opening angles, e.g. from γ conversion, which lead to poorly reconstructed decay vertices which pass the fiducial cuts. These are shown in Figure 1.5. The current vertex reconstruction is only based on the determination of the point at the minimum distance between the tracks. It is expected that a more sophisticated method with proper error determination will further increase the rejection power for such events. Work has started to make use of the Rave toolkit, a generic vertex reconstruction package developed by the CMS collaboration [2].

Background from electromagnetic interactions of muons has also been studied, i.e. interactions producing high energetic delta rays reconstructed as tracks. Although the currently available statistics is only corresponding to $\sim 2 \cdot 10^{15}$ protons on target, the events studied so far are easily rejected by a combination of fiducial cuts and veto cuts. This study will be continued with more statistics and with the vertex fitting implemented.

Table 1.6: Summary of the muon inelastic background events. Numbers correspond to 2×10^{20} protons on target. SBT = Surrounding Background Tagger (liquid scintillator), RPC = muon spectrometer of the ν_τ detector, UVT = Upstream Veto Tagger, SVT = Straw Veto Tagger.

	Number of candidates	$IP < 2.5\,\mathrm{m}$	$IP < 10\,\mathrm{cm}$
All (# tracks< 5)	1858.0	1136.0	14.0
From K^+	182.0	116.0	< 4.6
From K_S	52.0	36.0	< 4.6
From Λ	18.0	12.0	2.0
From K_L	422.0	278.0	2.0
From conv γ	342.0	236.0	< 4.6
	# tracks = 2		
Passing SBT	112.0	108.0	< 4.6
Passing RPC	16.0	< 4.6	< 4.6
Passing UVT	< 4.6	< 4.6	< 4.6
Passing SVT	< 4.6	< 4.6	< 4.6
Passing SVT&UVT&SBT	< 4.6	< 4.6	< 4.6
Passing SVT&UVT&SBT&RPC	< 4.6	< 4.6	< 4.6
using only Veto information of incoming muon			
Passing SBT	1424.0	916.0	10.0
Passing RPC	16.0	< 4.6	< 4.6
Passing UVT	1394.0	890.0	10.0
Passing SVT	1432.0	910.0	10.0
Passing SVT&UVT&SBT	< 4.6	< 4.6	< 4.6
Passing SVT&UVT&SBT&RPC	< 4.6	< 4.6	< 4.6
using only Veto information from particles produced in muon interaction			
Passing SBT	112.0	108.0	< 4.6
Passing RPC	28.0	10.0	< 4.6
Passing UVT	40.0	26.0	< 4.6
Passing SVT	< 4.6	< 4.6	< 4.6
Passing SVT&UVT&SBT	< 4.6	< 4.6	< 4.6
Passing SVT&UVT&SBT&RPC	< 4.6	< 4.6	< 4.6

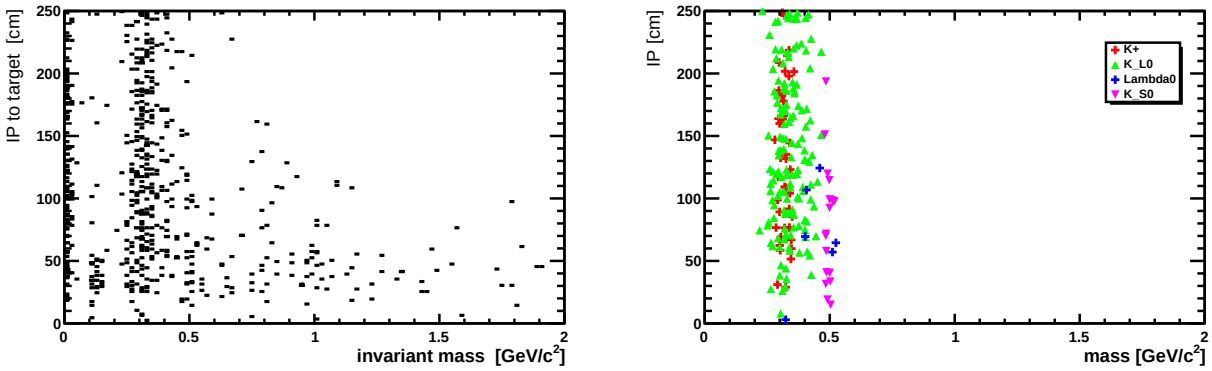

Figure 1.2: IP versus invariant mass for muon inelastic background events after requiring the number of reconstructed tracks in the event < 5 and no veto. Left: All combinations, Right: Combinations made from V^0 decay products.

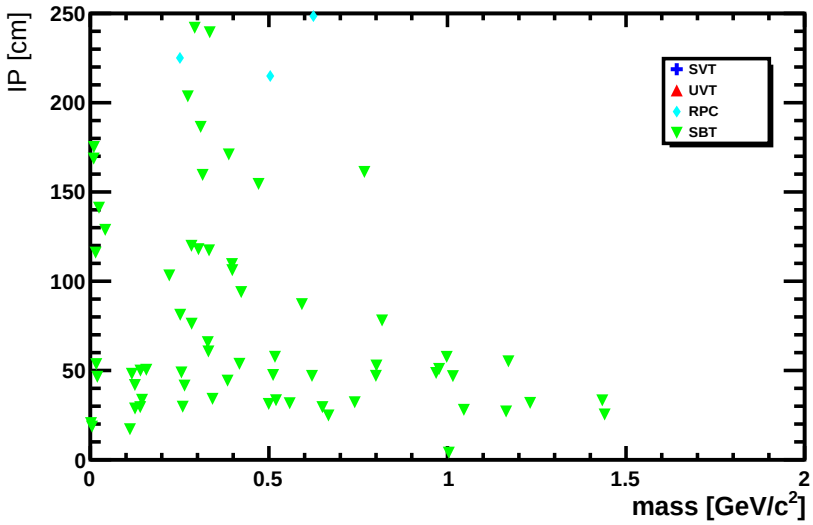

Figure 1.3: IP versus invariant mass of muon inelastic background events with two reconstructed tracks not vetoed by the veto detectors. Since the muons are entering from the front side, the Surrounding Background Tagger (SBT) has the smallest rejection power. The Straw Veto Tagger and the Upstream Veto Tagger reject all events, as shown in Table 1.6.

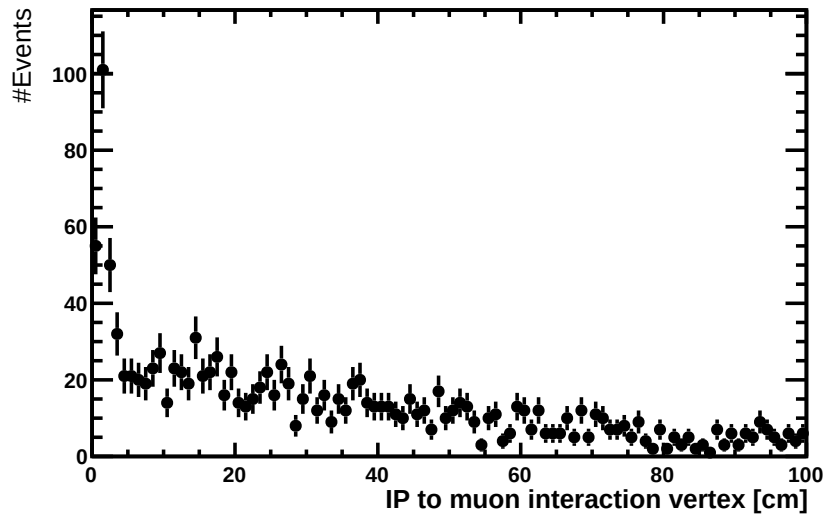

Figure 1.4: Impact parameter of reconstructed tracks with respect to the true muon interaction point.

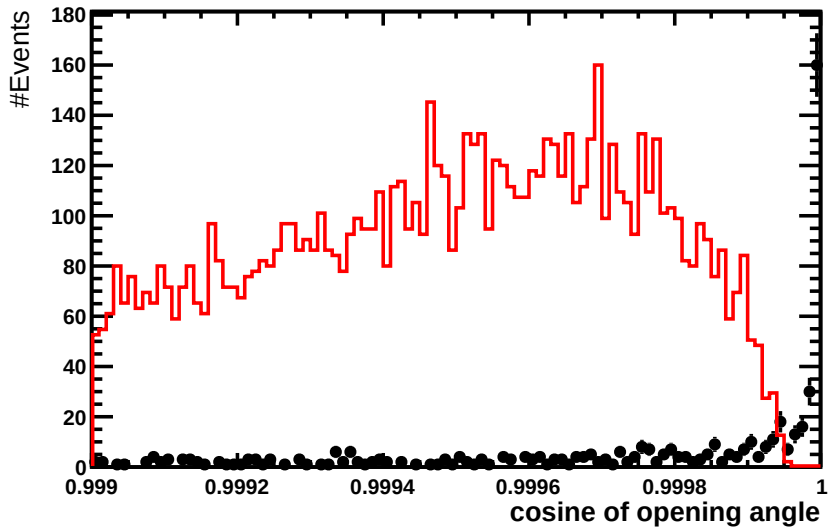

Figure 1.5: Opening angle between the two tracks forming a vertex in the fiducial volume, red is signal from $\mu\pi$ decays of HNLs with mass 1 GeV/c^2, black is background.

1.4 Muon combinatorial background

Muon combinatorial background has been described in the TP. We roughly expect a rate of 50 kHz muons with a momentum larger than 1 GeV/c entering the detector and a rate of about 7 kHz of muons with a momentum larger than 3 GeV/c.

It is impossible to produce $2{\cdot}10^{20}$ protons on target in full simulation. Therefore a dedicated fast simulation was prepared to evaluate the rejection of this background. The fast simulation was tuned against the full FairSHiP simulation of the equivalent of $6{\cdot}10^{10}$ protons on target. Comparisons between the full and the fast simulations are shown in Figure 1.6 for representative variables.

In addition, a sample of purely combinatorial muons is obtained by mixing two muons from two different HNL signal candidates simulated with FairSHiP. The resulting distributions of the vertex position of the combinatorial candidates and the impact parameter to the target are shown in Figure 1.7. Reasonable agreement is observed between this sample and the fast simulation used to generate the combinatorial background. The gives confidence that the fast simulation reproduces well the distributions and that it is relatively immune to the true p_{T} spectrum of the muons.

The combinatorial muons are randomly distributed over the whole length of the spill, hence the most effective way to reject them is using a coincidence requirement based on the timing detector. Assuming a rate F, the probability to find a muon in a time interval ΔT is $p_\mu = F \times \Delta T$. The probability to find two muons in the same time interval $p_{\mu\mu}$ is obtained using a Poisson distribution with mean p_μ. For $F = 50$ kHz and $\Delta T = 340$ ps we find $p_{\mu\mu} \sim 1.4 \cdot 10^{-10}$. In order to get the number of combinatorial muons $N_{\mu\mu}$ in five years of data taking we have to multiply this number by the number of buckets 340 ps long which we will have in $5 \cdot 10^6$ spills, $N_{\mathrm{buckets}} = 1.5 \cdot 10^{16}$. Hence we get $N_{\mu\mu} = p_{\mu\mu} \times N_{\mathrm{buckets}} \simeq 2 \cdot 10^6$.

In general, muon combinatorial background events have good quality tracks but they do not have a vertex reconstructed in the fiducial volume and they do not point to the target. For this reason the selection based on kinematic and fiducial cuts provides an additional rejection factor of $\sim 10^4$. In addition these events can be detected by the upstream veto and surrounding veto taggers. Assuming a tagger inefficiency of 1%, the probability of not seeing two muons is 10^{-4}. This implies that the expected number of background events is $2 \times 10^6 \times 10^{-4} \times 10^{-4} = 0.02$, which brings this background well below 0.1 events. This background requires a large safety factor since its rate depends quadratically on both the muon flux and the tagging inefficiency.

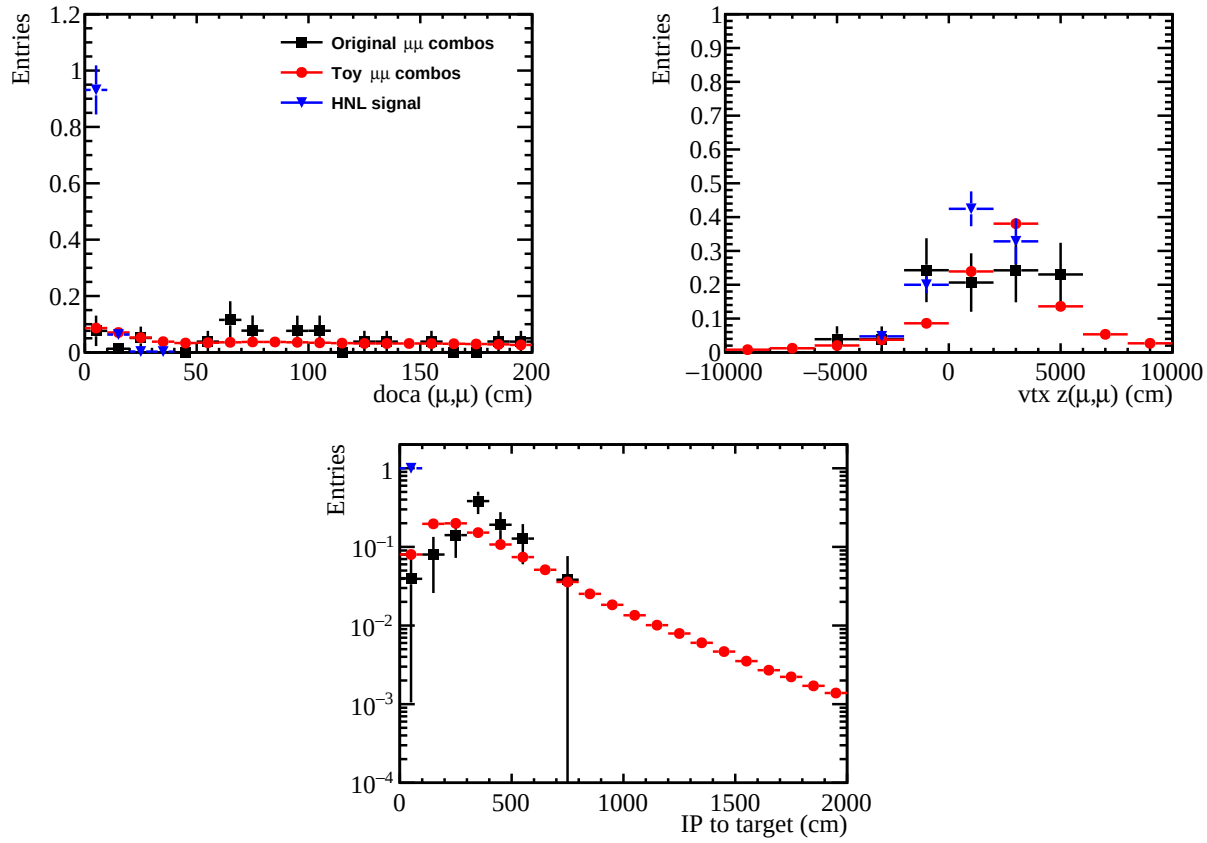

Figure 1.6: Comparison between the full simulation and fast simulation for combinatorial background.

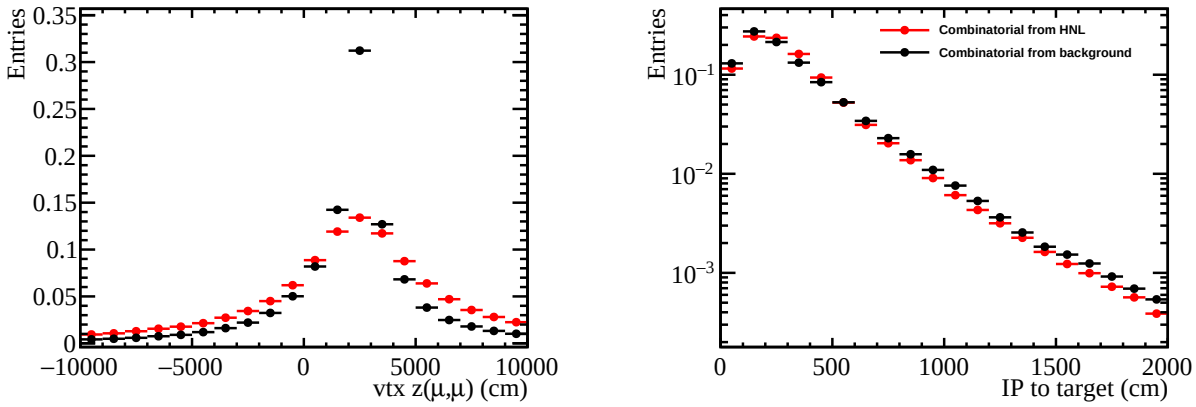

Figure 1.7: Comparison between the fast simulation for the combinatorial background and a sample of combinatorial muons obtained mixing muons from signal HNL decays.

1.5 Cosmics muon background

The background associated with cosmic rays is mainly due to muon inelastic scattering in the vicinity of the decay volume. Muons from cosmic rays are generated to reproduce the measured flux at sea level of 174 $m^{-2}s^{-1}$ [3]. As a result, $3.2{\cdot}10^3$ cosmic rays are expected to cross the detector every spill, hence 1.6×10^{10} during the data taking of $2{\cdot}10^{20}$ protons on target in nominal conditions.

In this study we increased the sample used for the TP by a factor 2 for muons with $p > 100$ GeV/c and by a factor 10 for muons with $p < 100$ GeV/c. The statistical weight factor is therefore $w = 1600$ for background events with $p > 100$ GeV/c and $w = 2$ for $p < 100$ GeV/c.

The topology of this background is such that the requirement of having two reconstructed tracks of opposite charge and good quality in the HS spectrometer already brings to a rejection factor of $\sim 6 \times 10^{-7}$. The requirement of having a vertex with DOCA$<$ 10 cm (hence a factor of ten times larger than the standard cut) further reduce this background down by a factor 20. The remaining events have all $IP > 33$ m with respect to the target, hence they all would be cut away by the requirement of having $IP < 2.5$ m. Another rejection factor of 10^{-2} comes from the requirement of having no hits in the surrounding veto tagger.

Table 1.7 shows the upper limit at 90% CL for the cosmics background along with the statistical weight in the two momentum intervals.

Table 1.7: Upper limit at 90% CL on the number of cosmics muon background events as derived from the full simulation. The sample is divided in two momentum ranges.

Bkg source	Stat. weight	Expected background (U.L. 90% CL)
μ Cosmics ($p < 100.0$) GeV/c	2.0	1.2
μ Cosmics ($p > 100.0$) GeV/c	1600	0.002

1.6 Background summary

The impact parameter (IP) at the target is one of the most effective variable in rejecting neutrino and muon induced backgrounds. For fully reconstructed signal events the IP distribution has an RMS of about 1 cm while for the partially reconstructed signal events it is much broader but still sufficiently narrow to provide good discrimination against background. Figure 1.8 (left) shows the IP distribution for the decay $HNL \to e^+e^-\nu$ with a mass of 100 MeV/c^2 and for the decay $HNL \to \mu^+\mu^-\nu$ with a mass of 1 GeV/c^2.

The background has in general a much broader distribution, as shown in Figure 1.8 (right, black curve). Moreover the events with small IP are those produced in the interactions with the material in front of the decays vessel. They are efficiently rejected thanks to the redundancy of the veto systems in the upstream direction. As shown in Figure 1.8 (right, red curve), the IP distribution becomes almost flat after applying the veto criteria.

The most effective criteria to reject the muon combinatorial background is a combination of veto tagging at least one of the two incoming muons and the requirement from coincidence,

which together provides a reduction factor of $\sim 10^{-9}$. Events induced by interactions of cosmic muons with the detector material are easily rejected using just kinematic and fiducial requirements.

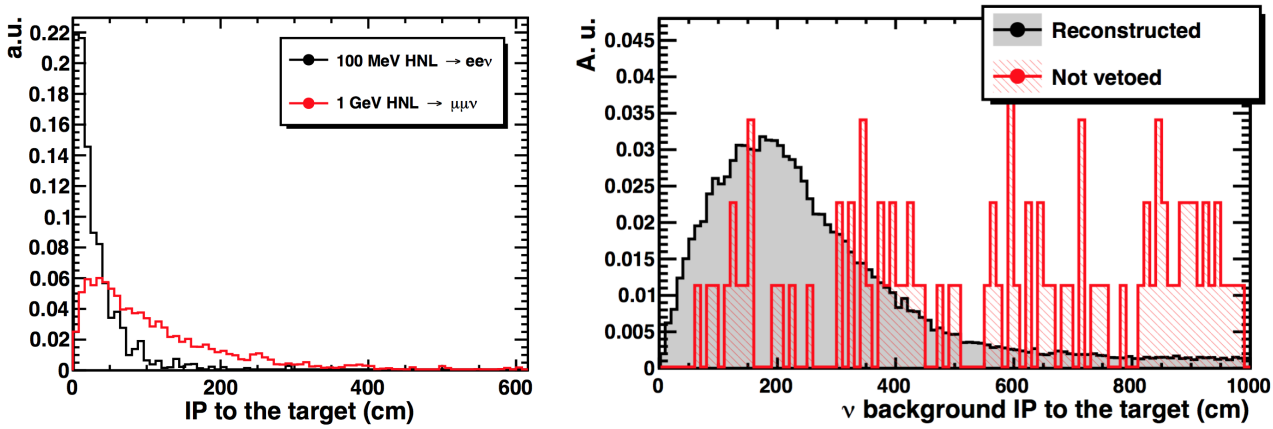

Figure 1.8: Left: IP distribution for the decay $HNL \to e^+e^-\nu$ with invariant mass of 100 MeV/c^2 (black) and for $HNL \to \mu^+\mu^-\nu$ with invariant mass 1 GeV/c^2 (red). Right: IP distribution for neutrino background. The black curve is for neutrinos induced background with at least two reconstructed tracks in the detector, the red curve is for neutrino induced background with at least two tracks and not vetoed.

Table 1.8 summarizes our current knowledge of the contamination from various background components. Some background components have different statistical weights for different momentum bins. In all cases the weights have been sizably increased with respect to the TP. After applying the fiducial, kinematics, timing and veto requirements, we are left with zero events for all the backgrounds. Hence we set upper limits at 90% CL according to $UL(90\%\text{CL}) = -\ln(0.1)/\text{weight}$.

In conlusion, based on the current understanding of the different backgrounds. All of them can be efficienctly rejected thanks to highly redundant selection criteria. The upper limits are expected to further decrease with increased Monte Carlo samples.

Table 1.8: Background yields for different background sources. The weight is the ratio between the generated sample and the expected yield for $N_{\rm pot} = 2 \cdot 10^{20}$. In all cases, zero events remain after applying all the selection criteria. Hence, an upper limits at 90 % CL is calculated as UL(90%) $= -\ln(0.1)/\text{weight}$. For the muon inelastic background, the upper limit is conservatively calculated by ignoring the factorizability of the veto efficiencies for the incoming muon and for the particles produced in the muon interaction. Assuming the factorizability suppresses this background by another factor 10^3.

Background source	Stat. weight	Expected background (UL 90% CL)
ν-induced		
$2.0 < p < 4.0$ GeV/c	1.4	1.6
$4.0 < p < 10.0$ GeV/c	2.5	0.9
$p > 10$ GeV/c	3.0	0.8
$\overline{\nu}$-induced		
$2.0 < p < 4.0$ GeV/c	2.4	1.0
$4.0 < p < 10.0$ GeV/c	2.8	0.8
$p > 10$ GeV/c	6.8	0.3
Muon inelastic	0.5	4.6
Muon combinatorial	–	<0.1
Cosmics		
$p < 100$ GeV/c	2.0	1.2
$p > 100$ GeV/c	1600	0.002

1.7 Impact of the background on the sensitivity for HNL

The following evaluates the impact of having a background of 10 events (a factor $\times 100$ more than expected) on the HNL sensitivity, as an example. It is assumed that this background is known with a systematic uncertainty of 60%, hence $N_{\text{bkg}} = 10 \pm 6$. Figure 1.7 shows the sensitivity with 0.1 background events, which is the targeted level of background, and with 10 ± 6 background events. The impact, even in this pessimistic scenario, is quite marginal as compared to the significant improvement on the limits from previous experiments. It is worth noting that in this estimate, the invariant mass is not used as an additional selection criteria in order to stay model independent.

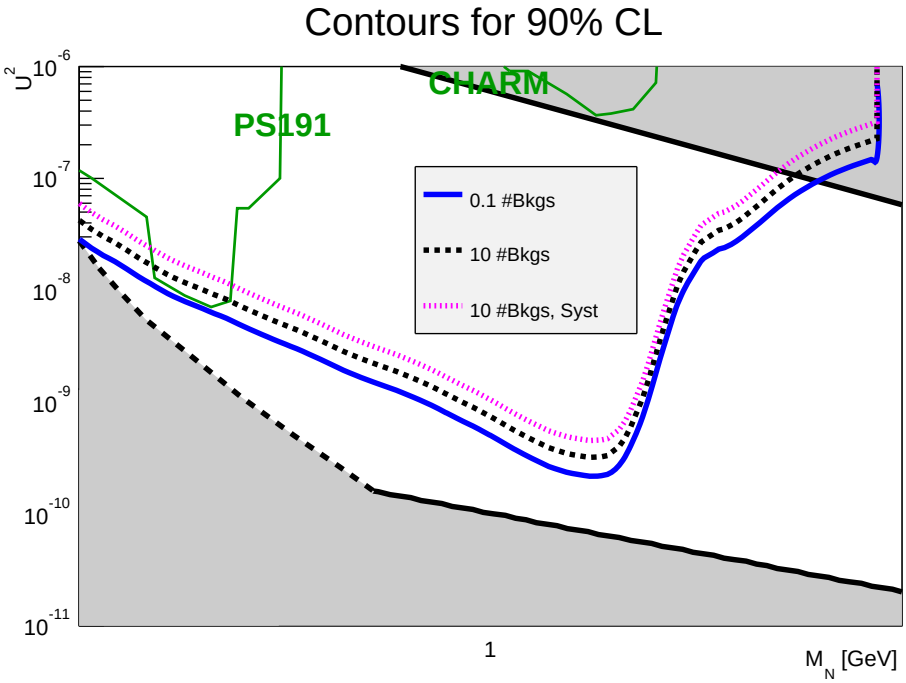

Figure 1.9: Sensitivity plot with the 90% CL upper limit for HNLs. The blue curve is assuming 0.1 background events in $2 \cdot 10^{20}$ protons on target. The dashed black curve corresponds to 10 background events and the solid black curve is for 10 ± 6 background events.

Chapter 2

Updated signal sensitivities

Since the TP the signal yields have significantly increased for both dark photons produced in QCD reactions and in neutral meson decays, and for all hidden particles produced in decays of charmed and beauty hadrons. The production yield of dark photons was strongly underestimated in the TP due to a trivial error in the calculation of the equivalent luminosity. The updated sensitivity for dark photons is shown in Section 2.2.

For the production of hidden particles (HNLs, dark scalars, axions, sgoldstino, neutralino, etc) in decays of charm and beauty hadrons, the cross-sections of the $c\bar{c}$ and $b\bar{b}$ events are now corrected for a significant contribution from cascade production. The cascade production will also increase the yield of tau neutrinos in the same manner since they are predominantly produced in the decay chain of D_s mesons.

Moreover, the signal yields (see equation 5.1 of the TP [1]) in the TP were estimated using the total cross-section. Since the elastic cross-section is ~ 17 % of the total cross-section, the yields should be increased by ~ 20 % by using the non-elastic cross-section instead. A toy-study based on Pythia 6.205 has been carried out to estimate the increase in yield, including all secondary interactions.

All sensitivity plots will be updated once these effects have been implemented in the full MC.

For all background calculations the interactions of secondaries in the target, and in all material following the target, including concrete walls of the hall, were already fully taken into account in the Geant4 simulations.

2.1 Contribution to the signal yields from secondary interactions in the target

2.1.1 $\chi(pp \to c\bar{c})$

Figure 2.1 shows the ratio $R_{c\bar{c}} = \frac{\chi_{c\bar{c}}}{\chi_{c\bar{c}}(400\ \text{GeV p})}$, for protons, neutrons, pions or kaons. The curves are parametrizations using a few $\sqrt{s}$ points simulated with Pythia. The larger ratio for mesons is due to their smaller total cross-section as compared to protons/neutrons.

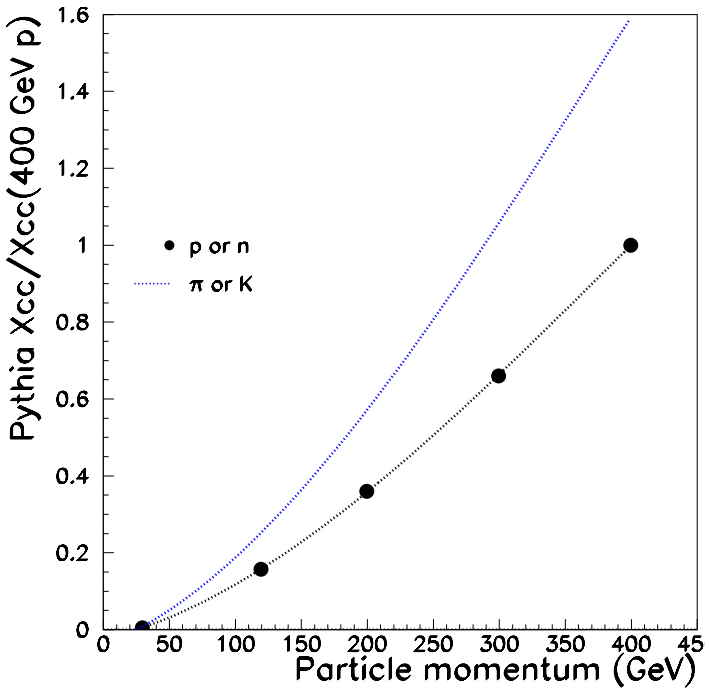

Figure 2.1: Parametrizations of the ratio $\frac{\chi_{c\bar{c}}}{\chi_{c\bar{c}}(400\ \mathrm{GeV\ p})}$ for protons, neutrons, pions or kaons.

Pythia is used to generate pp interactions, and for every interaction the parametrization as shown in Figure 2.1 is used to estimate the contribution of secondaries to $\chi_{c\bar{c}}$. Figure 2.2 shows $\Sigma R_{c\bar{c}}$ per event, taking only $p,\ n,\ \pi$ or K into account. The peak around $\Sigma R_{c\bar{c}} = 1$ corresponds to elastic and diffractive contributions. The total increase in charm production is expected to be ~ 61 %, in which secondary proton or neutron interactions account for ~ 48 %. The small tail with $\Sigma R_{c\bar{c}} > 1$ is due to very large momentum pions produced in diffractive interactions, in combination with the larger fraction of $c\bar{c}$ production in πp interactions compared to pp interactions which have a larger total cross-section.

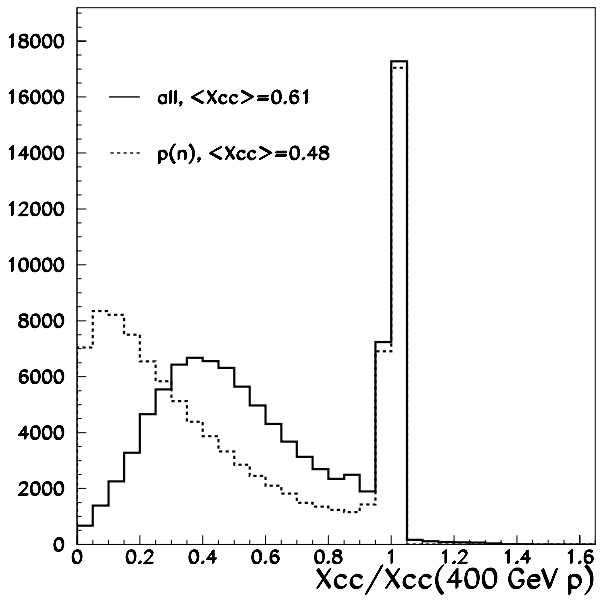

Figure 2.2: $\Sigma R_{c\bar{c}}$ per event, taking only $p,\ n,\ \pi$ or K into account.

2.1.2 $\chi(pp \to b\bar{b})$

The $b\bar{b}$ production at relatively low $\sqrt{s}$ is dominated by $q\bar{q}$ fusion, contrary to $c\bar{c}$ production which is dominated by gg-fusion. As a consequence, meson beams result in a much larger $\sigma_{b\bar{b}}$ than proton beams. Figure 2.3 shows selected [4] measurements of $\sigma_{b\bar{b}}$ compared to values obtained with Pythia 6.205. Pythia gives $\sigma(\pi^{-(+)} \to b\bar{b}X) = 9.0(3.4)$ nb, in comparison with the WA92 data which gives $5.7 \pm 1.5 \pm 1.3$ nb for 350 GeV π^-Cu [4]. Hence this gives confidence in using Pythia for parametrizing the cross section as a function of momentum of the incident mesons and baryons. For obtaining $\Sigma R_{b\bar{b}}$ per event the same procedure as above for $\Sigma R_{c\bar{c}}$ is followed.

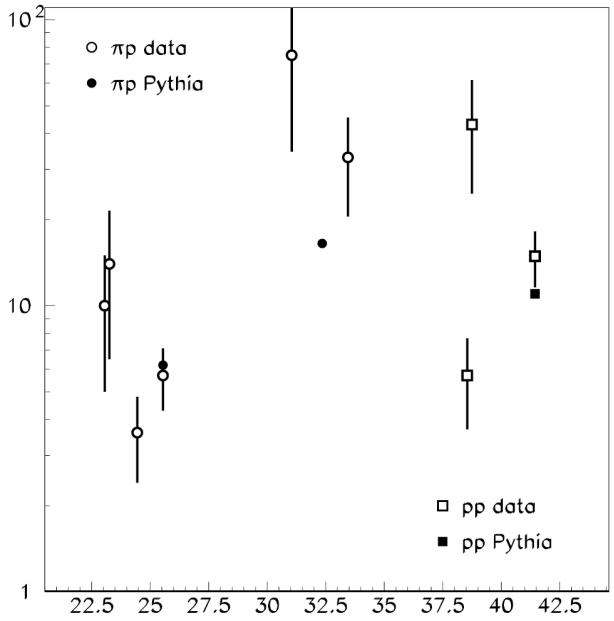

Figure 2.3: Measurements of $\sigma_{b\bar{b}}$ compared to Pythia 6.205.

Figure 2.4 shows the ratio $R_{b\bar{b}} = \frac{\chi_{b\bar{b}}}{\chi_{b\bar{b}}(400\ \mathrm{GeV\ p})}$ and $\Sigma R_{b\bar{b}}$ per event.

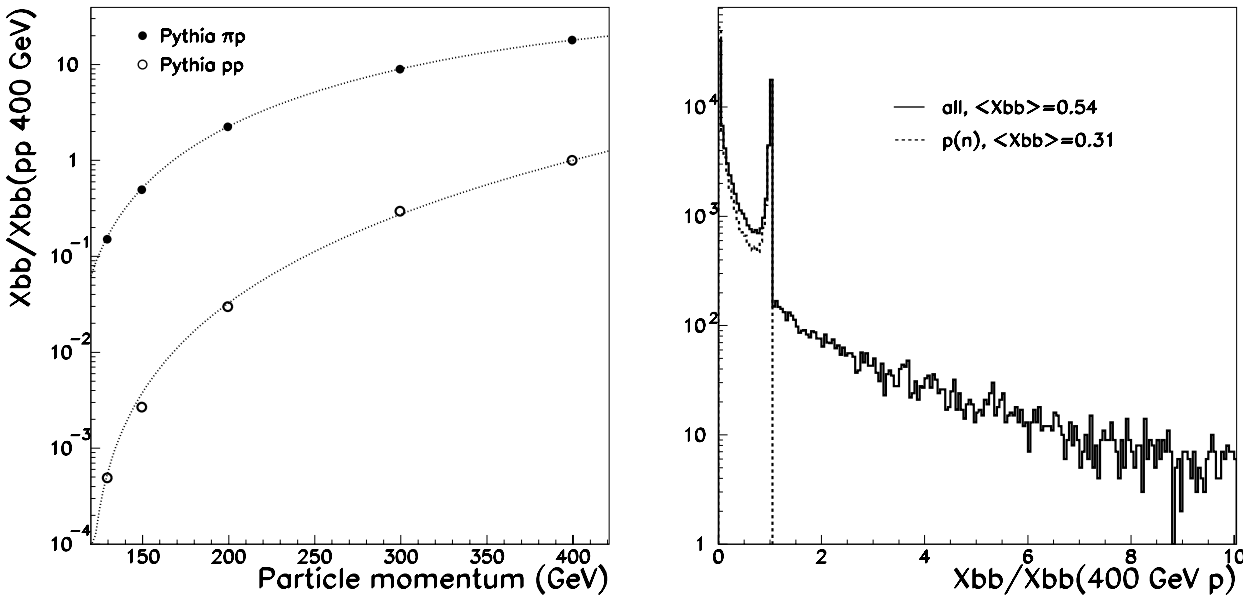

Figure 2.4: Parametrizations of the ratio $\frac{\chi_{b\bar{b}}}{\chi_{b\bar{b}}(400\ \mathrm{GeV\ p})}$ for protons, neutrons, pions or kaons shown in the left panel. The right panel shows $\Sigma R_{b\bar{b}}$ per event.

The total increase in beauty production is expected to be $\sim$ 54 %, in which secondary proton or neutron interactions account for $\sim$ 31 %.

2.1.3 Signal acceptance from cascade production

The majority of the extra charm and beauty hadrons produced in the cascade will have momenta smaller than the promptly produced charm or beauty leading to larger production angles for the hidden particles. The production of hidden particle in the decays of these secondary heavy hadrons has not yet been implemented in the full signal Monte Carlo. However, the corresponding loss of acceptance has been estimated for cascade production of HNLs using a toy MC which simulates the lower momenta charm and beauty decays, their corresponding HNL production angle, and imposing the SHiP acceptance.

While the increase in the number of $c\bar{c}$ is expected to be ~ 61 %, the corresponding increase in detected HNLs with a mass of 1 GeV/c^2 is expected to be ~ 48 %. The increase in the number of $b\bar{b}$ is expected to be ~ 54 %, which corresponds to an increase in detected HNLs with a mass of 2.5 GeV/c^2 of ~ 43 %. Note that both these numbers include the 20 % increase from the use of the non-elastic total cross-section for calculating the yield.

2.2 Updated efficiencies for HNLs and Dark Photons

Tables 2.1 and 2.2 summarize the selection efficiencies for the HNL signal ($HNL \to \pi\mu$) and for the Dark Photon $\gamma' \to \mu^+\mu^-$ signals, respectively, using the selection criteria listed in Section 1.1. The Dark Photon $\gamma' \to \mu^+\mu^-$ can be considered as an excellent approximation also for the Dark Scalar $\to \mu^+\mu^-$ decay.

Table 2.1: Efficiencies corresponding to different selection criteria for the $HNL \to \pi^+\mu^-$ decay. The efficiency of each cut is computed with respect to the preceding cut.

Selection	**Entries**	**Acceptance**	**Selection efficiency**
Event reconstructed	4471	6.43×10^{-6}	-
1 HNL candidate	4386	6.27×10^{-6}	97.6 %
Vtx in fiducial vol.	3777	5.37×10^{-6}	85.7 %
Tracks in fiducial vol.	3508	4.77×10^{-6}	88.8 %
N.d.f. > 25	3345	4.45×10^{-6}	93.2 %
DOCA < 1 cm	3161	4.15×10^{-6}	93.3 %
χ^2/N.d.f. < 5	3161	4.15×10^{-6}	100.0 %
Daughters $P > 1$ GeV	3160	4.15×10^{-6}	99.9 %
IP < 0.1 m	3137	4.11×10^{-6}	99.1 %
Event not vetoed	2969	3.91×10^{-6}	95.1 %

Figure 2.5 shows the update of the sensitivity to Dark Photons which replaces Figure 2.6 in the Physics Paper. The updated sensitivity includes both the updated efficiencies shown in Table 2.2, and the corrected calculation of the equivalent luminosity.

Table 2.2: Efficiencies corresponding to different selection criteria for the $\gamma' \to \mu^+\mu^-$ decay. The efficiency of each cut is computed with respect to the preceding cut.

Selection	**Entries**	**Acceptance**	**Selection efficiency**
Event reconstructed	59222	2.51×10^{-16}	-
1 γ' candidate	58211	2.5×10^{-16}	99.5 %
Vtx in fiducial vol.	50160	2.16×10^{-16}	86.4 %
Tracks in fiducial vol.	46600	2.13×10^{-16}	98.7 %
N.d.f. > 25	44519	2.1×10^{-16}	98.6 %
DOCA < 1 cm	41799	2.01×10^{-16}	95.8 %
χ^2/N.d.f. < 5	41799	2.01×10^{-16}	100.0 %
Daughters $P > 1$ GeV	41752	2.01×10^{-16}	100.0 %
IP < 0.1 m	41477	2×10^{-16}	99.7 %
Event not vetoed	39457	1.89×10^{-16}	94.3 %
1 muon in 1$^{\text{st}}$ muon station	39225	1.88×10^{-16}	99.7 %
1 muon in 2$^{\text{nd}}$ muon station	38780	1.87×10^{-16}	99.4 %

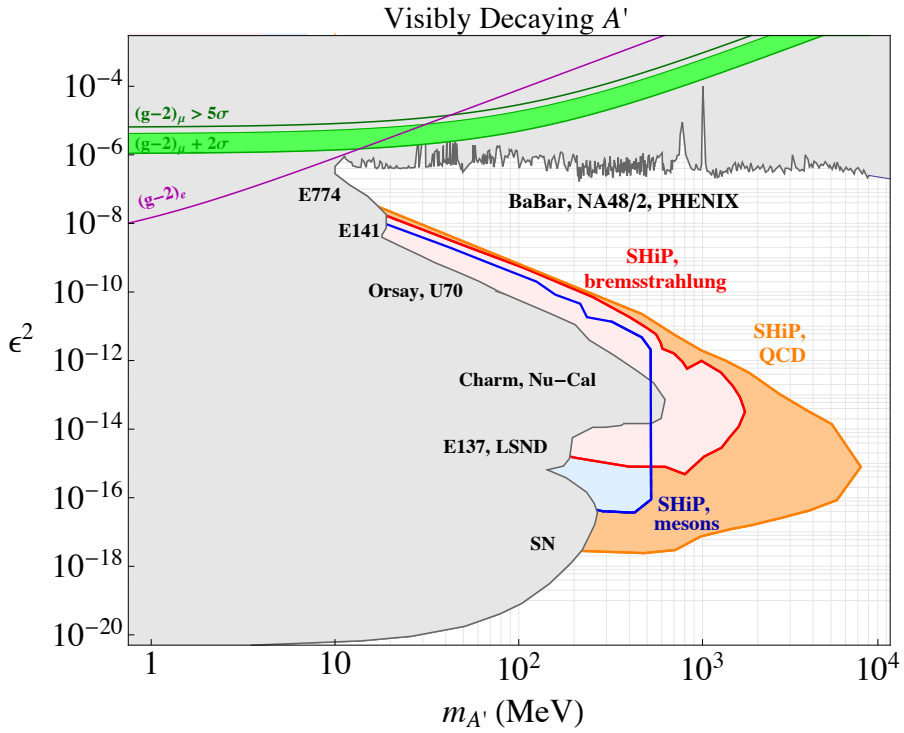

Figure 2.5: Updated sensitivity to dark photons. This figure replaces Figure 2.6 of the SHiP Physics Proposal.

Chapter 3

Comparison of the SHiP sensitivities with CERN, FNAL and JPARC beams

LBNE can use their 7 m long Near Detector (ND) to search for HNLs [5], and they estimate a factor seven improvement in yield compared to the results from CHARM. The geometry of the ND hall would allow a maximal decay length of about 30 m. The expected number of signal events in this configuration exceeds by about a factor of 200 the number of events in CHARM, The sensitivity curve has been shown in Figures 4.10 and 4.11 of the SHiP Physics Proposal [6]. This should be compared to the roughly five orders of magnitude increase of yield in SHiP compared to CHARM.

The ν-beam of LBNE excludes building a SHiP-like detector closer to the target than is foreseen for their ND. However, for the purpose of comparing the extreme case it is assumed here that both FNAL and CERN decide that the search for HNL-like particles is the highest priority in the next decade, i.e. both FNAL and CERN will dedicate their protons to a SHiP-like experiment.

The number of protons on target for SHiP (see section 3.1 in the SHiP TP [1]) assumes that 20% of the SPS physics time is devoted to the LHC. The remaining time is shared between SHiP with $4 \cdot 10^{19}$ protons on target per year, and the other NA experiments, which receive about 10^{19} protons on target per year. Dedicating 80% of the SPS physics time to SHiP alone would increase the number of protons on the SHiP target to $8.5 \cdot 10^{19}$/year.

FNAL will deliver $1.1 \cdot 10^{21}$ protons on target per year at 120 GeV. This is achieved with a 10 μs extraction in a 1.2 s long cycle. The short spill increases the combinatorial background by ten orders of magnitude. For the purpose of comparing equivalent conditions, it is assumed that a slow extraction is developed to provide a spill length of 1 s, as used for SHiP. This reduces the FNAL protons on target to $5.9 \cdot 10^{20}$ per year. As a result, FNAL produces seven times more protons on target that CERN in these conditions.

Using a toy MC it is estimated that the length of the active muon shield can be reduced by 25 m with a 120 GeV proton beam due to the lower momentum of the muons.

In parallel to these studies, the physics requirements of the production target design and its feasibility at FNAL and JPARC was investigated [7]. Based on the available material data and assuming the same design as the SHiP target and of the beam sweep, the envisaged scenario at the SPS is the safest from the point of view of the target operation and radiation damage, and leaves most margin to the limits of the material properties. The scenario at FNAL with $5.9 \cdot 10^{20}$

protons on target per year at 120 GeV ($7.5{\cdot}10^{13}$ pot every 2.4 s) is at the limit of feasibility and its operation appears unsafe due to the modification of the mechanical properties, especially the tensile strength, as a result of the radiation damage. The scenario at FNAL with $1.5{\cdot}10^{14}$ protons on target every 2.4 s at 120 GeV and the scenario at JPARC with $5{\cdot}10^{14}$ protons on target every 2 s at 30 GeV is excluded due to the excessive temperature reached by the target plates. A completely new concept for a high power target, most likely requiring a lower Z material, would be needed to cope with those beam parameters.

Comparison CERN-FNAL: HNL yield

The optimal length of the decay volume at FNAL is 40 m for 1 GeV/c^2 HNL particles produced in semi-leptonic charm decays. Hence, at FNAL the spectrometer can be positioned 31 m closer to the target compared to SHiP. Assuming a SHiP-like spectrometer with the same $5 \cdot 10$ m^2 elliptical transverse shape, the toy MC shows that per produced HNL the acceptance ratio FNAL/CERN=0.6 due to the lower longitudinal momentum of the produced particles.

The ratio of charm cross-sections was calculated with the program MCFM [8] at parton level, including NLO QCD. This yields a ratio of $\sigma(c\bar{c})$ FNAL(120 GeV)/CERN(400 GeV)=0.16. The total cross-section ratio for pp collisions is 0.95. Hence, six times more HNLs are produced at CERN per proton on target. As explained above, a factor of seven in favour of FNAL comes from the number of protons on target. Putting all factors together ($0.6 \times 0.16/0.95 \times 7$) shows that the yield at FNAL would be ~ 70 % of that at CERN.

Comparison CERN-FNAL: dark photon yield

The most sensitivity reach for dark photons comes from their production in QCD reactions as shown in Figure 2.5 The comparison between SHiP, and possible experiments at FNAL and JPARC is shown in Figure 3.1. SHiP has slightly better mass reach due to the higher energy of the proton beam at the CERN SPS.

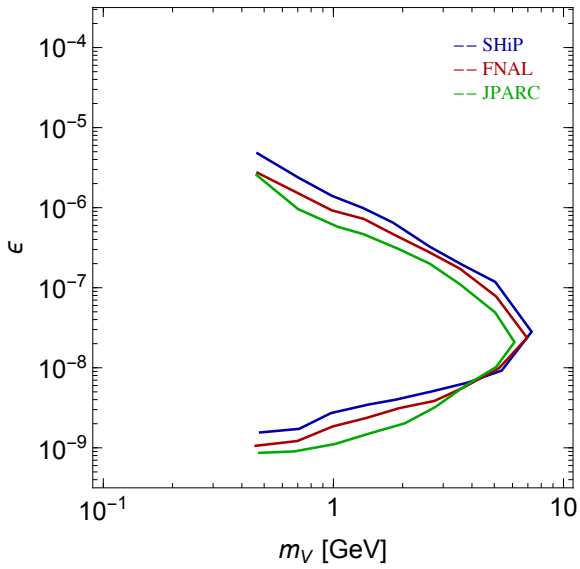

Figure 3.1: Sensitvity to Dark Photons from QCD production: SHIP@CERN , @FNAL; @JPARC

Comparison CERN-FNAL: dark scalar yield
Similarly to the charm, the ratio of beauty cross-sections was calculated with the program MCFM at parton level, including NLO QCD. This yields a ratio of $\sigma_{b\bar{b}}$ (FNAL(120 GeV)/CERN(400 GeV))=0.0016. Assuming $N_{\rm pot}$(FNAL) = $5.9 \cdot 10^{20}$ per year and $N_{\rm pot}$(CERN) = $8.5 \cdot 10^{19}$ per year, $\sim$ 100 times more dark scalars are produced per year at the CERN SPS.

The ratio of the acceptances FNAL/CERN has been computed using a toy MC assuming a coupling parameter of y^2 10^{-9} and a mass of the dark scalar of 1 GeV/c^2. Assuming the same parameters for the cross-section of the vacuum vessel and the distance to the target as for the comparison of the HNL yield, the acceptance ratio acc(FNAL)/acc(CERN) = 0.25. The lower acceptance at FNAL is due to the larger polar angle of the final decay products. Putting all the factors together, the yield of dark scalar coming from b decays at FNAL would be $\sim$ 400 times lower than that at the CERN SPS.

Comparison CERN-FNAL: ν_τ and $\overline{\nu_\tau}$ yields

The yield of events with ν_τ charged current interactions at the CERN SPS exceeds that at FNAL by a factor of 7. The uncertainty on the expected number of events for the determination of the F_5 structure function is significantly larger at FNAL, as shown in Figure 3. The top plots show the tau neutrino energy distribution at CERN (left) and at FNAL (right) including their uncertainty. Bottom plots report the variable r, defined as the ratio between the tau neutrino cross-section in the hypothesis of null F4 and F5 structure functions and in the SM case. The evidence for a non null value of F4 and F5 with a significance of 3σ requires the ratio to be larger than 1.6 for CERN and about 2.4 for FNAL. This makes the energy range where the experiment would be sensitive to those structure functions much narrower in the FNAL case, with an overall reduced sensitivity.

Comparison CERN-FNAL: cost
A detailed cost estimate as a function of the geometrical dimensions of the SHiP experiment will be done for the Technical Design Report. However, assuming for the time being that the costs of the active muon shield and the vacuum vessel scale linearly with their lengths, the cost reduction in building SHiP at FNAL would be about 40% for the active muon shield and 16% for the vacuum vessel, at the price of losing 30% of HNLs from charm, 99.75% of dark scalars from b decays, and 86% of $\nu_\tau, \overline{\nu}_\tau$.

Comparison CERN-JPARC
At JPARC the number of protons on target per year is $\sim$ 60 times larger than at the CERN SPS, but $\sigma(c\bar{c})$ at 30 GeV is a factor 200 smaller, and no beauty is produced. Hence, no toy MC study is needed to do the full comparison for HNL-like production and decay. It should be noted however that the parameter space covered for Dark Photons is very similar for a SHiP-like experiment at the CERN and JPARC.

Comparison with other competing experimental programmes
Using neutrinos produced in Z^0 decays, FCC-ee or ILC based experiments will extend the SHiP sensitivity to higher HNL masses, as shown in Figures 4.10 - 4.12 of the SHiP Physics Proposal. At the ILC the beam is dumped after each collision providing a platform for the design of an experiment to search for dark photons produced through the bremsstrahlung mechanism. Figure 3.3 shows the sensitivity of such an experiment with one year of running,

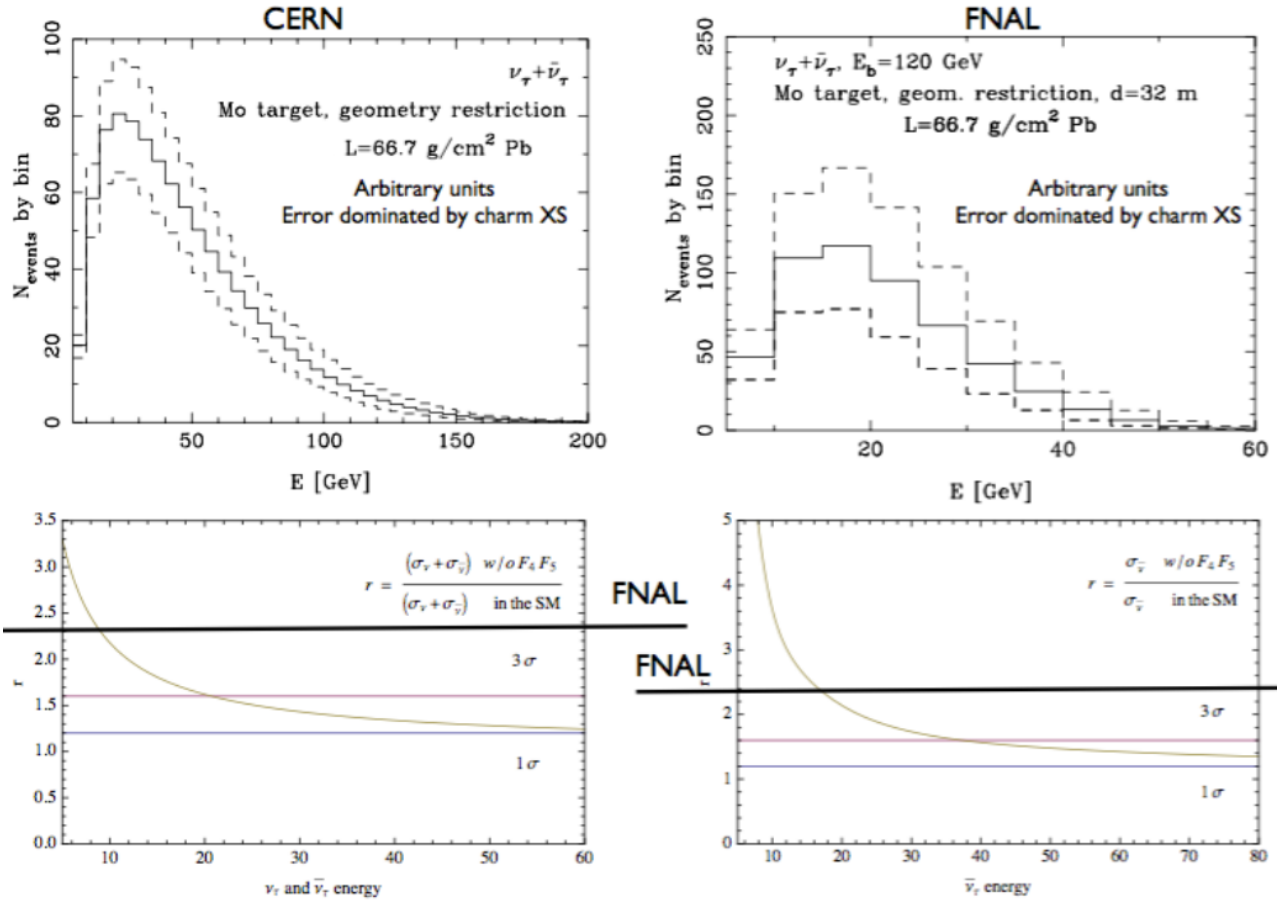

Figure 3.2: Tau neutrino energy distribution and its uncertainty at CERN (top left) and at FNAL (top right). The sensitivity to the F_5 structure function is restricted to a much more limited energy range at FNAL compared to CERN, thus being overall less sensitive.

assuming no background.

The Dark Light, HPS and APEX experiments at the Jefferson laboratory are planning to search for dark photons at lower masses. The expected sensitivities are shown in Figure 3.4.

For invisible decays of dark photons, electron beam dump experiments and Belle 2 could provide constraints similar to SHiP provided that the background level is close to zero. The SHiP sensitivity remains unique in lepto-phobic decay modes.

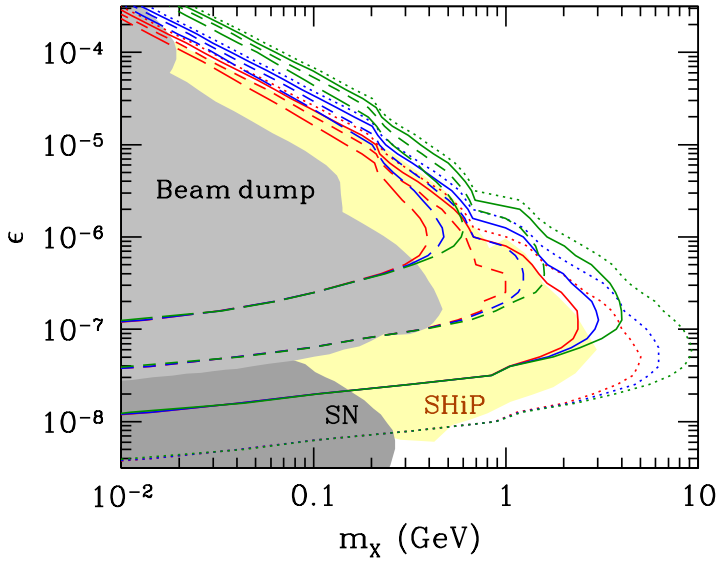

Figure 3.3: Contours of constant N_{sig} on the m_X vs. ϵ plane for $E_{\text{beam}} = 250$ (red), 500 (blue), and 1500 GeV (green), taking $N_e = 4 \cdot 10^{21}$, $L_{\text{dump}} = 11$ m, $L_{\text{sh}} = 50$ m, and $L_{\text{dec}} = 50$ m. The dotted, solid, short-dashed, and long-dashed lines correspond to $N_{\text{sig}} = 10^{-2}$, 1, 10^2, and 10^4, respectively. The gray-shaded regions are already excluded by past beam dump experiments [9] (light-gray) or supernova bounds [10] (dark-gray), while SHiP will cover the yellow-shaded area.

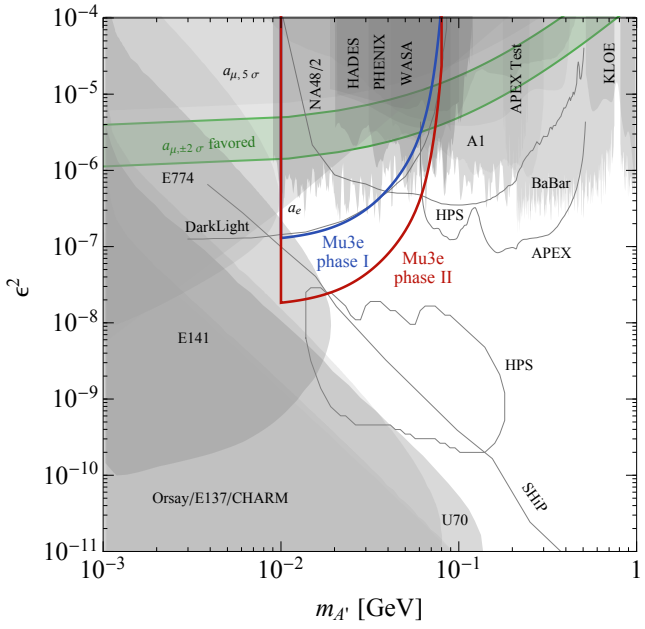

Figure 3.4: Sensitivity of experiments competing with SHIP on the search for dark photons decaying to visible products.

Chapter 4

Project Planning and Resources

4.1 Project schedule

The schedule presented in the SHiP Technical Proposal was based on the long-term accelerator schedule as it was defined at the time of writing the TP. The schedule was prepared taking into account the timeliness of the physics case, the time required to develop and build the detector and the facility, and minimal interference to the operation of the existing facilities at CERN. The choice of location of the facility was also taking into account these criteria. In addition the SHiP schedule aimed at allowing for a commissioning run of the facility and background measurement at the very end of Run 3 to ensure efficient start of the operation after LS3.

This leads to ten years between the Technical Proposal and start of data taking as soon as the SPS resumes operation after LS3. The ten years consist globally of three years for the comprehensive design studies as discussed below and the preparation of the TDRs, about five years of civil engineering (CE) in parallel with four years for detector production and staged installation of the facility, and another two years of detector installation. Along these guidelines, the civil engineering of the facility is naturally divided into four quasi-independent work packages [12] (time required for CE works in parentheses):

- WP1 : Junction cavern + 70m beam line (21 months)
- WP2 : Rest of beam line (12 months)
- WP3 : Target complex (12 months)
- WP4 : Experimental facility (18 months)

In addition, WP1 requires a period of cool down after the stop of NA operation, which could be largely covered by a preceding ion run. WP1 also requires removal and re-installation of the services and the beam line along a 100-metre stretch of TDC2 increasing the total time required for WP1 to 24-27 months. The splitting of WP1 and WP2 has been defined by the distance at which civil engineering may be done in parallel with operation of the North Area. Consequently only WP1 has to be done during a stop of the North Area. None of the work packages has any interference with the operation of the SPS and the LHC at any time.

The recent decision to construct the HL-LHC cryo, power and RF caverns and the LHC linkage tunnels at point 1 and 5 during a prolonged LS2 has led to two consequences for the

long-term accelerator schedule (MTP 2016-2020 V1). The start of LS2 is now at the end of 2018 and will last 24 months plus recommissioning. In principle, this has relatively limited impact on the TP SHiP schedule as it would only relax the TDR phase and the construction of the facility, and still allow a commissioning run, and starting the SHiP data taking when SPS resumes operation after LS3 in 2026. The updated SHiP schedule is shown in Figure 4.1.

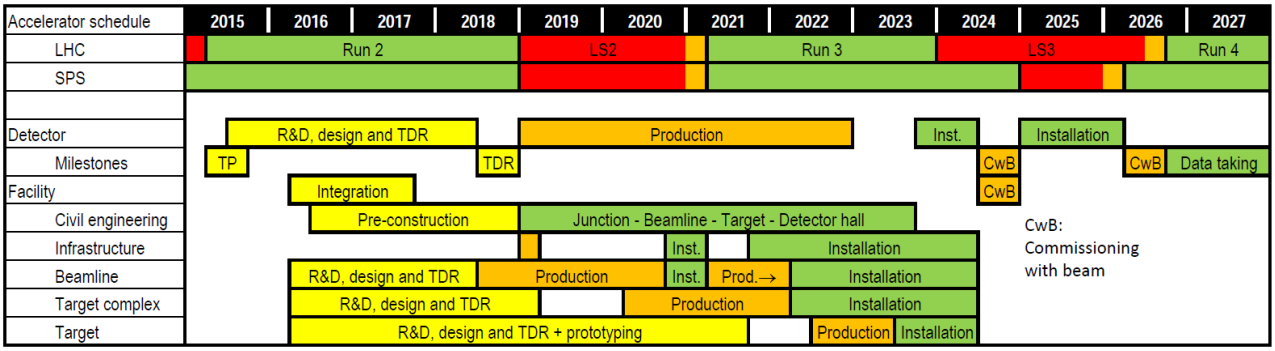

Figure 4.1: Updated project schedule for the facility and the SHiP experiment with the updated accelerator schedule as of MTP 2016-2020 V1.

However, it seems difficult to consider parallel civil engineering of the HL-LHC underground installations and the SHiP WP1, both for financial reasons and with the available CERN manpower. Therefore with the aim of avoiding overcommitment, a new schedule for the preparation of the SHiP facility has been prepared which still allows starting data taking at the beginning of Run 4 by reshuffling the order of the SHiP civil engineering work packages. The key change is the execution of WP1 during LS3. This only requires extending the stop of the North Area from currently one year to two years. The other work packages are naturally performed in the order WP3 - WP4 - WP2 to give more time for the most work intensive installations and in order to engineer the SHiP beam line and junction cavern in succession. Figure 4.2 shows this schedule assuming that the North Area is stopped in 2024 and 2025. Figure 4.3 shows the corresponding spending profile. Consequently, the latest start of the SHiP civil engineering assuming no parallel activities is the first half of 2021, which is after the peak activity of the HL-LHC underground civil engineering. This means that the preconstruction studies should start in the second half of 2018. In effect, this schedule relaxes significantly the initial phase and the overall preparation of SHiP, and it gives ample time for the installation of the target and the detector in fully completed facilities. The manpower allocation and the required funding for the design and implementation studies in 2016 - 2018 remains the same as before, as discussed below. The advantage of this schedule is that it allows decoupling completely the comprehensive design phase, the preparation of the TDRs, and all preconstruction activities from the construction and the production phase of the facility and the detector. The sole negative impact of this schedule is that it removes the possibility of a commissioning run before LS3. Consequently, the schedule shown in Figure 4.2 is now considered baseline.

In summary, the overall SHiP schedule of ten years from TP to data taking is driven by the technical challenges associated with the requirements of the largest possible number of protons on target and the extreme background suppression. At the same time, the above demonstrates that the schedule within the ten years is very flexible to accommodate financial constraints and

the availability of departemental resources, and to fit it into the global CERN strategy.

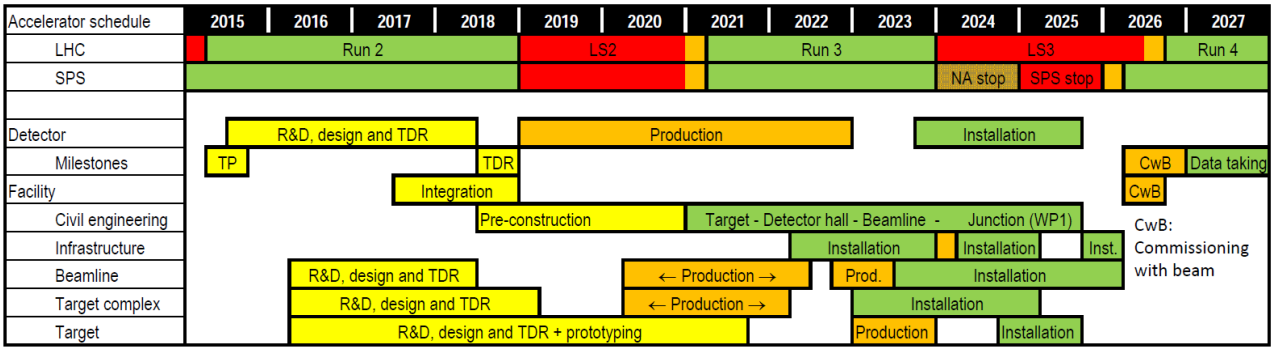

Figure 4.2: New baseline project schedule for the facility and SHiP experiment with WP1 in LS3 and adapted to latest accelerator schedule MTP 2016-2020 V1.

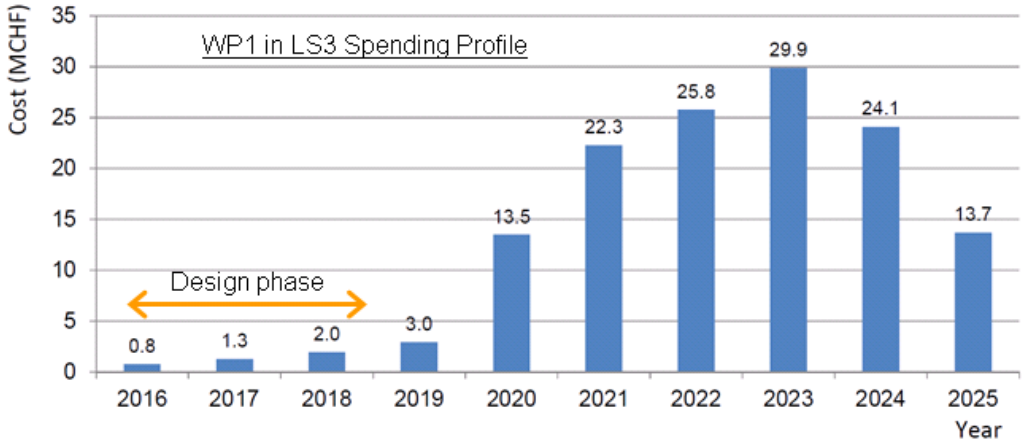

Figure 4.3: Overall cost profile for the construction of the facility in MCHF in the new baseline schedule with WP1 in LS3, as shown in Figure 4.2.

4.2 Facility-related studies and resources during the comprehensive design and preconstruction phases

The complementary documents to the TP in reference [12] - [16] describe all details of the implementation of beam line, the target, and radiation protection with the required R&D.

In the comprehensive design studies related to the beam transfer and the SHiP beam line, one critical item requiring R&D is the development of the three-way splitter switch that should serve the current COMPASS beam line and the other North Area targets, and the SHiP beam line in separate SPS cycles. The SHiP schedule with WP1 in LS3 relaxes significantly the development and production of this splitter/switch magnet. Secondly, the dilution of the beam

energy, as required by the target, should be ensured by a large beam spot and a large magnetic sweep of the beam on the target. These will be studied in detail, together with the critical interlocking and beam instrumentation required in TT20 and in the SHiP beam line. Apart from the development of the splitter/switch and the SHiP beam line, the performance and optimization of the SPS extraction is a critical item of study which will involve several SPS Machine Developments:

1. Setup and test of the SHiP cycle and one second extraction
2. Extraction losses and beam quality, including extraction septum performance limits
3. Spill uniformity
4. TT20 beam transfer for SHiP
5. New splitter/switch setup and performance

The second and the third studies are of high general interest beyond SHiP as they may allow reducing extraction losses and mitigating the radioactivation in SPS LSS2 (ALARA) and to improve on stability and reliability of the SPS extraction. This may also improve general beam quality and increase the yield for the North Area experiments. These studies will be complemented by the studies of alternative extraction techniques and crystal assisted extraction as studied within the UA9 project.

For the target, the prototyping including irradiation and material tests is expected to take four years. These studies will continue beyond the TDR. The comprehensive design studies for the target and the target complex will focus on the critical R&D aspects related to the target design including a study of an alternative He-cooled solution, the helium vessel and circulation, the shielding block design and optimization, in particular the support and the water plug-in system, etc. For the target material tests, external resources are being investigated to start this as early as possible.

The design studies related to the radiation protection of the facility are aimed at addressing accurately all aspects related to the shielding, dose monitoring, and work procedures, both during construction and operation of the facility. In particular, it will focus on the work procedures related to the demolition of TDC2 and the in-situ recycling of radioactive material, methods to mitigate the effects of radioactivation at the SPS extraction and intervention techniques, optimization of the target shielding, and verification of the doses around the detector along with the optimization of the muon shield and the finalization of the layout of the experimental facility.

A large number of these studies are in synergy with the general exploitation of the existing CERN facilities and developments of facilities at other labs.

The resources required[1] for the comprehensive design phase and the preparation of the TDRs related to the the facility is summarized as follows:

- Extraction, beam line and splitter/switch: 1.3 MCHF + 3 FTEs
- Target and target complex: 1.6 MCHF + 2.5 FTEs

[1] *FTE* is defined as the time required from one employee on a full-time basis to accomplish the task.

- Muon shield: 0.5 FTEs
- Radiation protection: 0.4 MCHF + 1.5 FTEs
- Safety engineering and environment[2]: 0.5 MCHF + 1.5 FTEs

This brings to a total of 3.8 MCHF and 9 FTEs required between 2016 and end of 2018.

While CERN is not directly committed to the development and construction of the muon shield, the vacuum vessel, and the two experimental magnets, it will be essential during the design phase to keep close contact with the CERN experts on aspects related to transport, in-situ construction, integration and safety of these items.

The preparatory phase for the SHiP civil engineering consists on the one hand of a relatively extensive integration study, and on the other hand of the preconstruction phase including core drilling, design, environmental impact assessment, construction permit, and tendering. The integration study for the facility will include representatives from the CV, EL, ABT, MEF, STI, RP, SEE, and CE groups, and is estimated to require 4 FTEs (the participation of the CE group is included in the resources for the preconstruction phase). The resources for the preconstruction phase is estimated to 2.7 MCHF, 5.5 FTEs of engineers and 3 FTEs of draughtsmen. In the original TP schedule updated with the changes to Run2/LS2, these resources have to be invested 2016 - 2018. In the new baseline schedule with WP1 in LS3, the resources may be made available two years later in the period 2018 - 2020.

In the original TP schedule, the critical work is related to WP1 to be executed during LS2. In total it amounts to 10 MCHF plus the resources required for the preconstruction phase as above. To begin the works efficiently at the start of LS2, 3.6 MCHF are required at the end of 2018. In the new baseline schedule with WP1 in LS3 shown in Figure 4.2, a similar amount gets shifted to the beginning of 2021.

4.3 Key milestones for the detector comprehensive design studies

The comprehensive design phase for SHiP does not require an extensive R&D since the detector is predominantly based on proven technologies. Instead it consists of a set of key milestones related to the optimization of the experiment and performance studies, followed by detailed technological implementation studies and prototyping. The key milestones with the highest priority concerns the layout of the experiment and the geometry of the detectors involving an overall re-optimization of the muon shield and the geometry of the decay volume, and revisiting the required vacuum pressure following the continued background studies with optimized detectors and number of readout channels etc. All of these offer possibilities for significant cost optimizations.

Table 4.5 shows the preliminary list of key milestones related to these critical studies. In addition, further re-optimization of the particle identication capability is to be expected. The milestones are prioritized and organized in order to limit the resource requests for 2016 without impacting progress. The milestones have been endorsed by the Collaboration as an

[2]Includes support for the detector design and implementation studies

appropriate basis for approaching funding agencies provided that the comprehensive design phase is approved by CERN. Table 4.1 shows the expected sharing of responsibilities for the comprehensive design phase.

Beam time in test beams will be important in 2016 to move ahead with the initial performance studies, and is expected to continue in 2017 and 2018.

In order to prepare for the TDRs, the comprehensive design phase will also address the other standard developments concerning the mechanics, electronics and infrastructure systems.

		2016				2017				2018			
	Key milestones	Q1	Q2	Q3	Q4	Q1	Q2	Q3	Q4	Q1	Q2	Q3	Q4
0	**Active muon shield**												
	Optimization of the field map for background suppression												
	Design of coil and yoke + optimization soft/GO steel, manufacturing method												
	Prototype construction and test												
	Study of (partially) superconducting option												
1	**Neutrino Target**												
	Optimisation of brick structure to separate electron anti-neutrinos/neutrinos												
	Optimization of ECC and CES mechanical assembly and target material												
	Demonstrate charge and momentum measurement in CES												
2	**Target Tracker (nTT)**												
	Demonstrate capability of connecting nTT and emulsion tracks at occupancy												
	Study and design of GEM, SciFi, Micromegas options												
3	**Muon Magnetic Spectrometer (nMMS)**												
	Test streamer mode operation for RPC at the design rates												
	Test OPERA RPCs for their possible re-use												
4	**Decay volume**												
	Study of the required vacuum pressure and optimal shape of decay volume												
	Design study including integration of surround scintillator, incl market survey												
	Study of alternative designs - concrete bunker												
5	**Surround Background Tagger (SBT)**												
	Optimization of liquid scintillator cell dimensions and PMT locations												
	Development of complete cell prototype with reflection paint and N flushing												
	Prototype performance tests												
6	**Upstream VETO Tagger (UVT)**												
	Performance tests of 4m scintillating bars												
	Optimization of the layout and support to minimize passive material												
	Prototype construction and test												
7	**Straw VETO Tagger (SVT)**												
	Background study to determine applicability and background rejection												
	Design study												

Figure 4.4: Key milestones per subsystem to be addressed during the comprehensive design phase.

		2016				2017				2018			
	Key milestones	Q1	Q2	Q3	Q4	Q1	Q2	Q3	Q4	Q1	Q2	Q3	Q4
8	**Spectrometer Straw Tracker (SST)**												
	Small-scale prototype construction and test												
	Demonstrate methods to control effect of straw sagging and alignment												
	Optimization of straw geometry, readout (1-, or 2-sided), overall geometry												
9	**Spectrometer magnet**												
	Definition of mechanical interface beteen HS magnet and vacuum vessel												
	Magnet design including mechanical analysis												
	Study of a superconducting alternative												
10	**Spectrometer Timing Detector (STD)**												
	Optimization of geometry, readout and mechanical support												
	Prototype construction and performance test												
	Demonstrate method of fine time alignment												
11	**Electromagnetic calorimeter (ECAL)**												
	Optimization of cell size and module structure												
	Demonstrate method of monitoring and calibration												
	Prototype construction and test												
12	**Hadronic calorimeter (HCAL)**												
	Optimization of cell size and module technology												
	Engineering prototype of HCAL												
	Development of monitoring system												
13	**Muon detector (MUON)**												
	Optimization of the general layout and dimensions of scintillating bars												
	Demonstrate the time resolution of 1ns												
	Full-size prototype construction and test												
14	**Online system**												
	Definition of the common readout protocol												
	TDAQ demonstrator performance evaluated												
	Readout control specification for the FE and the BE												

Figure 4.5: Continued, key milestones per subsystem to be addressed during the comprehensive design phase.

4.4 Update on the costs

The Collaboration has expressed interest in making use of the Goliath magnet. Since the availability of the Goliath magnet is not guaranteed at this stage, the comprehensive design phase will include the development of an alternative magnet as backup solution. As the geometry of the neutrino detector is involved in the overall performance and cost optimization of the experiment, the magnet is likely to have a significantly smaller width compensated by an increase in the vertical and the longitudinal size of the magnetic volume than Goliath to achieve the same performance of the neutrino target. For the purpose of completeness the cost of producing a re-optimized magnet has been estimated to 1 MCHF. The preliminary magnet design consists of a slim two-metre wide and four metre long magnet with a magnetic volume of W:1.0 x H:1.5 x L:3.0 m^3 and a horizontal 1 T peak field to ensure the momentum measurement in the Compact Emulsion Spectrometer. The power converter, interlocks and a cooling system which may also serve the Opera magnet have been estimated at 800 kCHF.

No attempt is made here to update the cost of the SHiP detector or the facility as a result of the optimizations discussed for the design phase.

Following an approval of the comprehensive design phase by the CERN committees, an MoU will be prepared covering the responsibilities for the detector construction. An indicative of the CERN contribution to the construction of the detector may be obtained by applying the same procedure as was applied in the LHCb MoU. According to the same rule, the current share of CERN authors would contribute to the construction with about 2 MCHF.

4.5 Update on status of Collaboration

Since the submission of the TP, the Gyeongsang National University (Korea) has joined the Collaboration. The National University of Science and Technology "MISIS" (Moscow) became an Associate Member hosted by the Lebedev Physics Institute RAS. Thus the Collaboration currently consists of 47 institutes in 15 countries with a total of 244 members. Several additional institutes have also expressed their interest in applying for Associate Membership.

Table 4.1: Interests expressed by the institutes in the construction of SHiP components.

Component	**Institutes**
Beamline and target	CERN
Infrastructure	CERN
Muon shield	RAL, Imperial College, Warwick, Bristol
HS vacuum vessel	NRC KI, NIKIET
HS spectrometer magnet	
Straw tracker	CERN, JINR, MEPhI, PNPI
ECAL	ITEP, Orsay, IHEP, INFN-Bologna
HCAL	ITEP, IHEP, INFN-Bologna, Stockholm
Muon	INFN-Bologna, INFN-Cagliari, INFN-Lab. Naz. Frascati, INFN-Ferrara, INR RAS, MEPhi
Surrounding background tagger	Berlin, LPNHE, MEPhI
Timing detector and upstream veto	Zürich, Geneva, INFN-Cagliari, Orsay, LPNHE
ν_τ emulsion target,	INFN-Naples, INFN-Bari, INFN-Lab. Naz. Gran Sasso, Nagoya, Nihon, Aichi, Kobe, Gyeongsang, Moscow SU, Lebedev, Toho, Middle East Technical University, Ankara
ν_τ target tracker	NRC KI, INFN-Lab. Naz. Frascati
ν_τ target magnet	
ν_τ muon spectrometer magnet	INFN-Bari, INFN-Naples, INFN-Roma
ν_τ tracking system (RPC)	INFN-Bari, INFN-Lab. Naz. Gran Sasso, INFN-Naples, INFN-Roma
ν_τ tracking system (drift tubes)	Hamburg
Online computing	CERN, Niels Bohr, Uppsala, UCL, YSDA, LPHNE
Offline computing	CERN, YSDA
MC simulation	CERN, Sofia, INFN-Cagliari, INFN-Lab. Naz. Frascati, INFN-Napoli, Zürich, Geneva and EPFL Lausanne, Valparaiso, Berlin, PNPI, NRC KI, SINP MSU, MEPhI, Middle East Technical University, Ankara, Bristol, YSDA, Imperial College, Florida, Kyiv

Bibliography

[1] SHiP collaboration, A Facility to Search for Hidden Particles (SHiP) at the CERN SPS, CERN-SPSC-2015-016, SPSC-P-350, 8 April 2015.

[2] URL: https://save.hepforge.org/

[3] . Kempa, J. and Krawczynska, A.", Low energy muons in the cosmic radiation, Nucl.Phys.Proc.Suppl., Vol. 151, pp. 299-302, 2006.

[4] C. Lourenco and H. Wohri, Heavy flavour hadro-production from fixed-target to collider energies, *Phys.Rept.* **433**, 127180, (2006).

[5] LBNE Collaboration, C. Adams et al., The Long-Baseline Neutrino Experiment: Exploring Fundamental Symmetries of the Universe, arXiv:±1307.7335.

[6] Alekhin, S. et al., Search for Hidden Particles, CERN-SPSC-2015-017, SPSC-P-350-ADD-1, 9 April 2015.

[7] M. Calviani, D. Horvath, A. Perillo-Marcone, V. Venturi, Considerations on the SHiP target at CERN, Fermilab and JPARC for the TP addendum to SPSC, EDMS: https://edms.cern.ch/document/1543159.

[8] URL: http://mcfm.fnal.gov/

[9] Andreas, S. et al., Hidden Photons in connection to Dark Matter, AIP Conf.Proc. 1563 (2013) 114-117.

[10] Kanemura, S. et al., Beam Dump Experiment at Future Electron-Positron Colliders, arXiv:1507.02809[hep-ph], 2015.

[11] R. Ball et al. [NNPDF collaboration], Nucl.Phys. **B809** (2009) 1-63, Nucl. Phys.**B816** (2009) 293.

[12] Manfredi, M. et al., Civil engineering for the SHiP facility, EDMS: https://edms.cern.ch/document/1499253 (SHiP-TP-2015-A6)

[13] Arduini, G. et al., The SPS beam parameters, the operational cycle, and proton sharing with the SHiP facility, EDMS: https://edms.cern.ch/document/1498984 (SHiP-TP-2015-A2)

[14] Goddard, B. et al., Extraction and beam transfer for the SHiP facility, EDMS: https://edms.cern.ch/document/1495859 (SHiP-TP-2015-A3)

[15] Calviani, M. et al., Design of the SHiP target and target complex, EDMS: https://edms.cern.ch/document/1465053 (SHiP-TP-2015-A4)

[16] Strabel, C. et al., Radiation protection studies for the SHiP facility, EDMS: https://edms.cern.ch/document/CERN-RP-2015-020-REPORTS-TN (SHiP-TP-2015-A5)